telecom

MDPI

*Article*

# Assessment of Electromagnetic Exposure to a Child and a Pregnant Woman Inside an Elevator in Mobile Frequencies

**Ioanna Karatsi [1], Sofia Bakogianni [2] and Stavros Koulouridis [1,*]**

[1] Department of Electrical and Computer Engineering, University of Patras, 26504 Patras, Greece; karatsi@upatras.gr
[2] School of Electronic Engineering and Computer Science, Queen Mary University of London, London E1 4NS, UK; s.bakogianni@qmul.ac.uk
* Correspondence: stavros.koulouridis@upatras.gr

**Abstract**

This study presents an in-depth dosimetry analysis of energy assimilation from EM waves and increase in the temperature during mobile phone usage within an elevator cabin. The cellphone operates at two different frequencies (1000 MHz and 1800 MHz) and is simulated at three different talk positions vertical, tilt, and cheek. Realistic numerical models of a woman in the third trimester of pregnancy and a girl at the age of 5 years are employed. The analysis highlights the necessity of a comprehensive approach to fully grasp the complexities of EM exposure.

**Keywords:** finite-difference time-domain (FDTD); realistic human body; pregnant woman model; Pennes equation; specific absorption rate (SAR); power absorption

## 1. Introduction

It is undeniable that the invention of the mobile phone was a turning point in modern history. It has offered people numerous advantages by bringing wireless communication into everyday life and allowing for immediate and continuous communication between people being some meters or hundreds of kilometers apart. Nowadays, it is an essential part of everyday life.

Since the first use of cell phones, extensive research is being conducted [1–12], because of the emitted electromagnetic energy, that has become an aspect of public issue of health and safety. Research studies were able to determine the relation of the rate of absorption energy with permittivity-related behavior, the spatial mass distribution, and the biological structure of the tissue itself, and also the power, the frequency, and the distance of the radiation source [13–21].

In several studies, the examination of specific absorption rate (SAR) is combined with temperature variations [22–28] to achieve a more holistic and detailed insight into the subject. As [29–34] suggest, it is essential to conduct thermal analysis alongside dosimetry analysis to gain a better understanding of the relationship between radiation from a mobile phone and human tissues.

While cell phones have become an integral part of daily routine, the age of their users is reduced, bringing forward the importance of electromagnetic microwave effects investigation by the scientific community at vulnerable population groups such as children [35–40], who might show greater sensitivity to EM exposure than adults [41–43]. And of course, high attention is paid to pregnant women [44–47] that should take extra care to be protected from the radio frequency [48,49].

check for updates

Received: 29 May 2025
Revised: 6 July 2025
Accepted: 11 July 2025
Published: 16 July 2025

**Citation:** Karatsi, I.; Bakogianni, S.; Koulouridis, S. Assessment of Electromagnetic Exposure to a Child and a Pregnant Woman Inside an Elevator in Mobile Frequencies. *Telecom* **2025**, *6*, 52. https://doi.org/10.3390/telecom6030052

**Copyright:** © 2025 by the authors. Licensee MDPI, Basel, Switzerland. This article is an open access article distributed under the terms and conditions of the Creative Commons Attribution (CC BY) license (https://creativecommons.org/licenses/by/4.0/).

Nowadays, wireless devices play a crucial role in daily tasks and activities, leading to their frequent use in enclosed spaces like transport vehicles and elevators [50–54]. In that sense, it is important to investigate real-life exposure scenarios of sensitive population groups in special environments. In this paper, we examine EM radiation exposure and heat-related distribution of a girl at the age of five and a woman in the third trimester of pregnancy inside an elevator cabin. In contrast with our prior work [55], in this research we changed the numerical humans' configurations in order to examine how exactly, and on which scale, the positioning of humans affects the quantities measured for all the utilized anthropomorphic phantoms, including the seven-month fetus. In order to explore how the fetus' measurements of thermal increase and electromagnetic absorption rate are affected by the child's body and if it plays a crucial role in the levels of electromagnetic exposure, we rotate the pregnant woman around eight different positions of the child with reference to the pregnant navel point. The pregnant-woman phantom was uniformly affixed at the umbilicus, selected as a consistent reference point across all experimental configurations, whereas in our previous investigation, the numerical Pregnant II model was centered within the metallic enclosure and subsequently rotated about its vertical axis through eight distinct orientations, each employing a different attachment point on the phantom. By employing a single attachment point that is chosen based on its provision of one of the highest exposure measurements in our prior work, we are able to isolate and evaluate the influence of varying handset–speaker positions relative to the maternal abdomen. This methodology permits a more precise assessment of how the measured parameters fluctuate with device placement, thereby enhancing our understanding of the positional effects of a child-held mobile phone model on fetal exposure.

SEMCAD-X software was used to carry out the dosimetry analysis [56], which relies on the finite difference time domain method for computation [57]. We used a numerical model of a cell phone [58] that operates at two frequencies of 1000 MHz and 1800 MHz and placed it at vertical, tilt, and cheek talk positions according to the standards of IEEE 1528 std and CENELECEN 62209 [59,60].

## 2. Specific Absorption Rate (SAR)

Concerning the exposure of humans to EM fields, guidelines have been established to prevent potential health risks. The parameter used to quantify these exposure limits is quantified by the Specific Absorption Rate (SAR), and it measures the rate at which biological tissues absorb electromagnetic energy deposited in biological tissue per unit mass. The spatial distribution of specific absorption rate is given by the following equation:

$$\mathrm{SAR} = \frac{\sigma \,|\, \mathrm{E} \,|^{2}}{\rho} [\mathrm{W/kg}] \tag{1}$$

where $\sigma$ $(\mathrm{Si/m})$ represents the tissue's electrical conductivity, $\rho\left(\mathrm{kg/m^3}\right)$ denotes the mass density of the biological tissue and E $(\mathrm{V/m})$ represents the effective induced electric field.

The specific absorption rate at the whole body is evaluated by the following equation:

$$\mathrm{SAR_{WB}} = \frac{\mathrm{P_{abs}}}{\mathrm{m}} [\mathrm{W/kg}] \tag{2}$$

where $\mathrm{P_{abs}}$(W) denotes the power that is absorbed, while m (kg) corresponds to the absorber's entire mass

According to international standards for safety, the maximum permissible spatial peak SAR, averaged over 10 g of biological tissue, is 2.0 W/kg, and the whole-body averaged SAR is constrained to 0.08 W/kg. These values are typically computed for a continuous exposure duration of 6 min [61,62].

## 3. Bioheat Equation and Boundary Conditions

The steady-state distribution of temperature in tissues is determined using the following Pennes bioheat equation [63]:

$$\rho c \frac{\partial T}{\partial t} = \nabla \cdot (k \nabla T) + \rho Q + \rho S - \rho_b c_b \rho \omega (T - T_b) \quad (3)$$

where $\rho\left(kg/m^3\right)$ represents the medium's density, c $(J/(kg{\cdot}^\circ C))$ is the specific heat capacity, T $(^\circ C)$ denotes the temperature of the tissue, t (s) refers to time, k $(W/(m{\cdot}^\circ C))$ indicates the efficiency of heat conduction within the tissue, Q $(W/kg)$ refers to the rate of metabolic heat generation, S $(W/kg)$ corresponds to specific absorption rate (SAR), $\omega\left(m^3/(kg{\cdot}s)\right)$ represents the rate of blood flow through tissue, $\rho_b\left(kg/m^3\right)$ is the density of the mass, $c_b$ $(J/(kg{\cdot}^\circ C))$ indicates the thermal capacity of the material, and $T_b$ $(^\circ C)$ is the heat level of blood [64].

When the bioheat equation is used in a simulation that aims to determine the temperature rise (Tincr) from SAR exposure, and SAR-induced temperature rises are expected to remain below 1 °C, all tissue and boundary parameters (ρ, c, k, ω, Q, $T_n$, h, and $T_b$) can be treated as temperature and time independent. We therefore write the total temperature as follows:

$$T = T_{base} + T_{incr}$$

Substitute into the following standard Pennes equation:

$$\rho c \frac{\partial T_{incr}}{\partial t} = \nabla \cdot (k \nabla T_{incr}) + \rho S - \rho_b c_b \rho \omega T_{incr} \quad (4)$$

The following boundary conditions were applied in this study to determine the temperature distribution [65,66]:

Mixed boundary condition:

$$k \frac{\partial T_{incr}}{\partial n} + h T_{incr} = 0 \quad (5)$$

where h denotes the coefficient of the heat transfer, $T_{incr}$ represents the rise in temperature, and n is the unit normal vector directed outward from the surface interface. Mixed boundary conditions were implemented at the tissue–air interfaces. The heat transfer coefficient (h) between the skin and the surrounding air was defined as $h_{skin\text{-}air} = 8\ \left(W/\left(m^2{\cdot}K\right)\right)$ and between the cornea and the external air h was set as $h_{cornea\text{-}air} = 20\ \left(W/\left(m^2{\cdot}K\right)\right)$ [65].

The boundary condition of Neuman:

$$k \frac{\partial T_{incr}}{\partial n} = 0 \quad (6)$$

The boundary condition of Neumann was enforced at the interfaces of biological tissues and air-filled cavities, covering the internal passages of the pharynx, bronchi, trachea, and esophagus.

The boundary condition of Dirichlet:

$$T_{incr} = 0 \quad (7)$$

The Dirichlet boundary conditions were defined at the interface adjoining the circulatory system that includes the veins, arteries, the umbilical cord and all the tissues that are surrounded by blood-perfused, excluding air-filled tissues, maternal and fetal cerebrospinal fluid (CSF), maternal and fetal vitreous humor, amniotic fluid, teeth, stomach lumen, and

the small intestine lumen. Additionally, the ambient external temperature was steady set to $T_{external}$ = 24 °C, and the human's temperature fixed at $T_{human}$ = 37 °C.

A non-uniform grid mesh was utilized, and the minimum grid resolution of 1 mm was applied in proximity to the source and within specific tissues of the anatomical phantoms of humans for both electromagnetic and thermal simulations. In the surrounding environment, representing free-space air, the maximum grid resolution was set at 30 mm for both considered frequencies. This resolution was achieved by adjusting the maximum step at the two frequencies, corresponding to the distinct wavelengths (λ) in free space, which are λ = 299.79 mm at 1000 MHz and λ = 166.67 mm at 1800 MHz. The full FDTD simulation computational domain encompassed between 46.5456 million and 116.345 million cells, depending on the specific simulation configuration and the operational frequency of the cellular device.

## 4. Models and Method

To compare with our previous work [55], we use the same computational humans from the Virtual Population (VP) [67] and the same mobile phone model [58]. Cell phone modeling and its performance are discussed in [55]. The anthropomorphic phantoms were selected in such a way that the height of the gestating woman's navel, the child's head, and the mobile phone edge source were at the same height. For simplification, we refer to the numerical female at the seventh month of gestation as Pregnant II and to the 5-year-old numerical child as Roberta.

We also kept the same metallic cabin elevator with the roof opening as in [55], following the standards set by Greek building legislation [68] and the regulations for ventilation at elevators [69] (Figure 1).

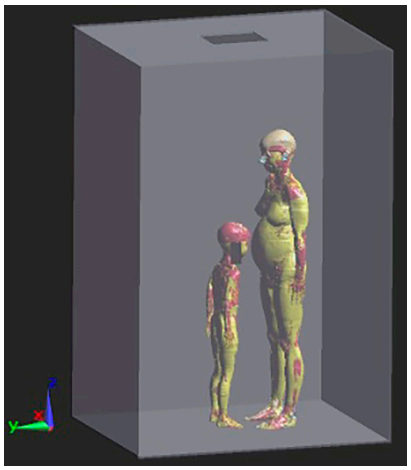


**Figure 1.** The numerical phantoms configuration 1: inside the metallic cabin of the elevator, with the cellular device positioned next to the right side of Roberta's head, at her ear place, aligned parallel.

Roberta is placed at the center of the metallic cabin, and the Pregnant II is placed at eight different configurations around Roberta with her navel as a connection point to each position; so that we can examine especially the fetus dosage by the emitted radiation at different explosion configurations. The portable device is aligned to Roberta's right ear (left area in the overhead view). The configurations of computational humans with more details are discussed below (see Figures 2 and 3).

The eight different configurations of the human models are shown in Figure 3. The configurations of the models were chosen so that the distances between them are minimum.

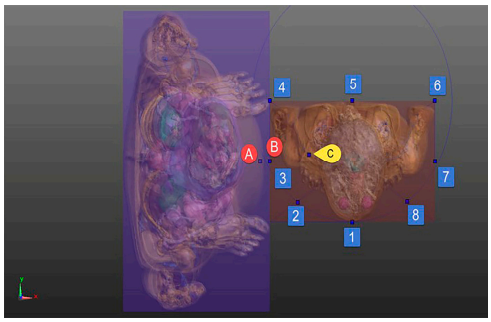



**Figure 2.** Points A, B, are the points of connection between the child and pregnant woman virtual humans (A fixed—navel point; and B each time the points 1 to 8), C is the wireless device source point.

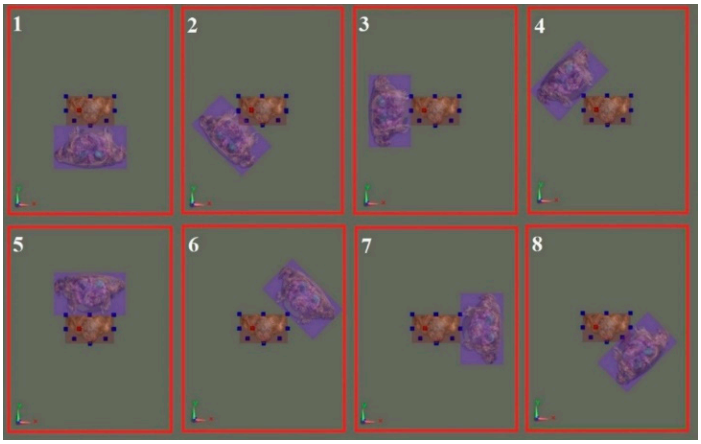



**Figure 3.** All eight configurations of the two virtual humans. The numbers 1–8 represent the phantom placement scenarios.

The portable device consistently remains on Roberta's right side and is positioned in three distinct talking configurations (see Figure 4), following the guidelines set by IEEE 1528 and CENELECEN 62209 [59,60] that is as follows: (a) aligned along the *z*-axis (parallel) (b) tilted with an angle relative to the *z*-axis (tilt), and (c) positioned near the cheek with angles relative to both the *z*-axis and *x*-axis (cheek).

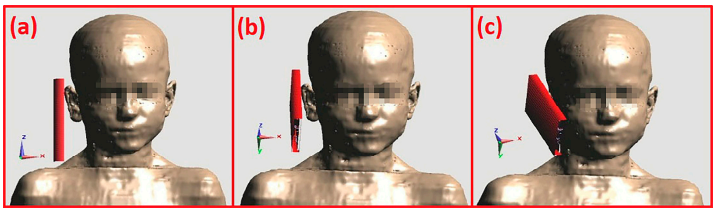



**Figure 4.** Handset placements relative to Roberta: (**a**) parallel, (**b**) tilt, and (**c**) cheek.

By following the IEEE Std 1528-2013 [70] instructions, we validated our measurement system using a flat phantom that eliminates the confounding effects of complex head geometries. The phantom comprises an inner liquid block (225 × 150 × 150 $mm^3$) whose dielectric properties mimic tissue ($\varepsilon_r$ = 41.5, $\sigma$ = 0.97 S/m at 1000 MHz; $\varepsilon_r$ = 40.0, $\sigma$ = 1.40 S/m at 1800 MHz) and a uniform 2 mm thick outer shell ($\varepsilon_r$ = 3.7, $\sigma$ = 0.0016 S/m at both frequencies). To evaluate positional sensitivity, we performed measurements in three phone-to-phantom configurations, always maintaining a 2 mm separation from the phantom surface: once aligned to the speaker aperture (the S-point), once to the geometric center of the phone's outer case, and once to the RF source point on the outer case. This consistent spacing and repeatable alignment ensure that any variation in the measured

fields reflects the device's radiation characteristics rather than differences in positioning or anatomy.

## 5. Results

For the two frequencies under consideration, 1000 MHz and 1800 MHz, the numerical results are presented individually for every figure. Average specific absorption rate over 10 g tissue mass, whole body energy absorption, and temperature increase are calculated at free space and at a closed area. For comparison reasons, we kept the same format of presentation as [55]. Additionally, electromagnetic dose rate over 10 g and thermal rise surface images of the pregnant woman are provided for the phone position where their maximum values were observed. Pin, the input power, is assigned a value of 1 W.

### *5.1. Specific Absorption Rate over 10 g (SAR10g) and Temperature Variations*

#### 5.1.1. Cell Phone Transmission Frequency of 1000 MHz (SAR10g &Tmax)

For the model Roberta, electromagnetic deposition rate over 10 g measurements and thermal variations at 1000 MHz are shown in graphical form at Figure 5.

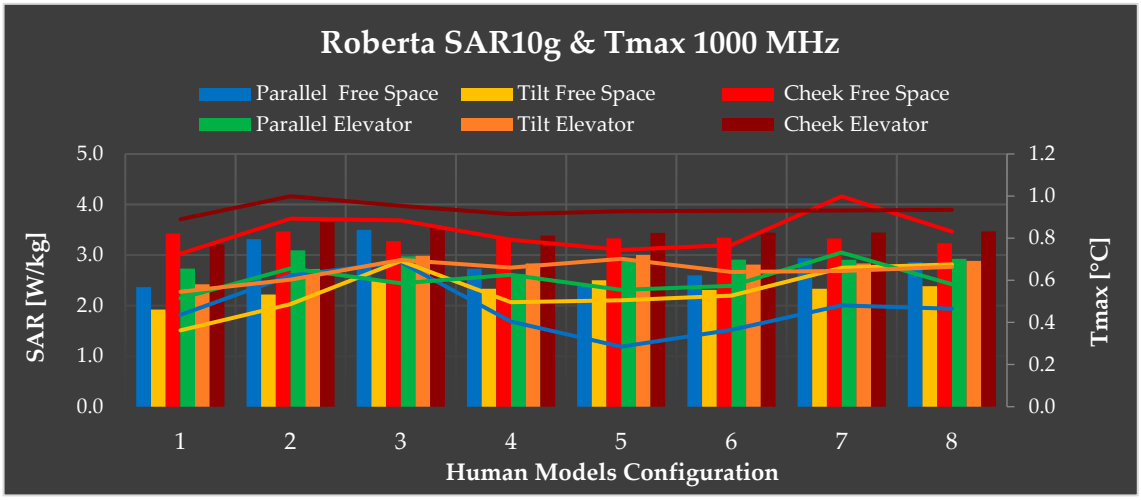



**Figure 5.** Chart display of SAR10g [W/kg] and peak temperature increase (Tmax) [°C] values in the Roberta model at 1000 MHz with the cellphone operating at an output power of 1 W. Eight different anatomical phantom setups and three mobile phone placements, inside an elevator and at open space were assessed. The bar graphs indicate specific absorption rate values, whereas the line plots represent temperature data.

The data analysis shows the greatest specific power density over 10 g value inside the elevator cabin, which is observed at the cheek phone position for configuration, while the minimum is recorded at the tilt phone position (configuration 1 of Figure 5). In free space, the highest specific dose rate over 10 g occurs at the vertical orientation of the cellular device for humans in configuration 3, and the lowest is found at the tilted phone orientation (configuration 1 of Figure 5).

Regarding the induced temperature rise (Tmax), the maximum value within the elevator is observed at the cheek phone position (configuration 7), and the minimum occurs at the tilt phone position (configuration 1). In free space, the maximum Tmax is recorded at the parallel phone position (configuration 7 of the models), while the minimum is observed at the parallel phone position (configuration 5).

The tissue absorption intensity over 10 g and the peak temperature increase in the seventh month pregnant woman (Pregnant II) and the fetus at the 1000 MHz are presented in Figures 6 and 7, respectively.

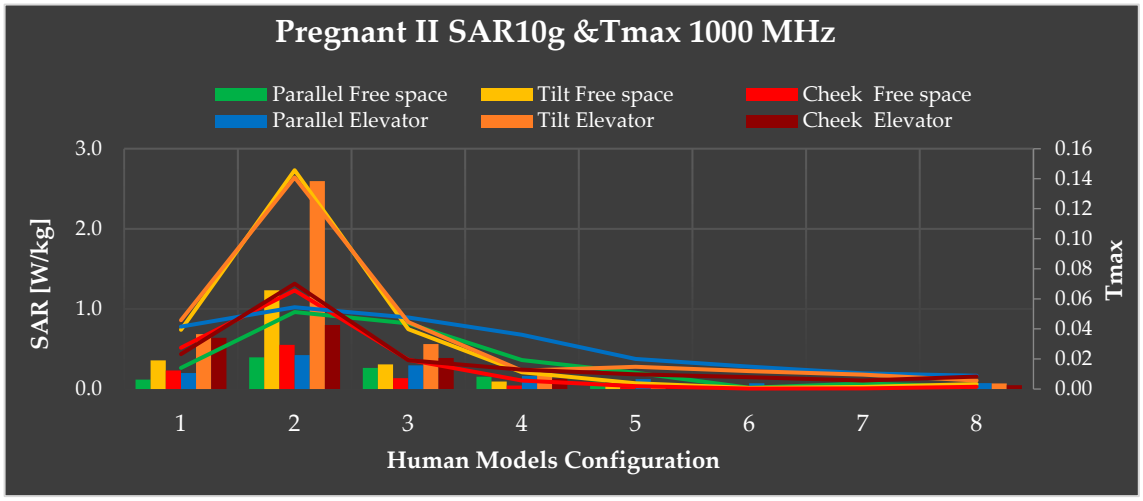



**Figure 6.** Chart display of SAR10g [W/kg] and peak temperature increase (Tmax) [°C] values in the Pregnant II model at 1000 MHz with the cellphone operating at an output power of 1 W. Eight different anatomical phantom setups and three mobile phone placements, inside an elevator and at open space were assessed. The bar graphs indicate specific absorption rate values, whereas the line plots represent temperature data.

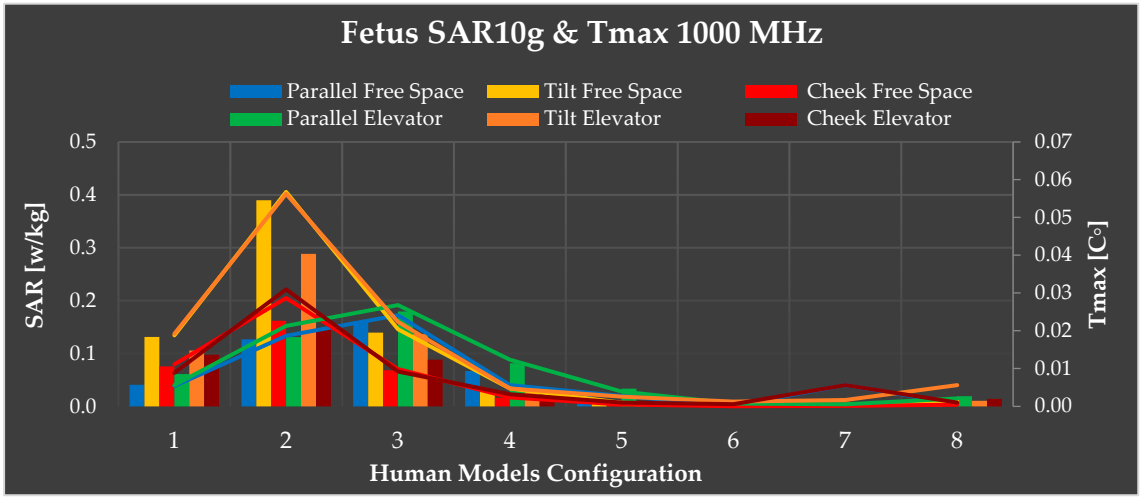



**Figure 7.** Chart display of SAR10g [W/kg] and peak temperature increase (Tmax) [°C] values in the fetus model at 1000 MHz with the cellphone operating at an output power of 1 W. Eight different anatomical phantom setups and three mobile phone placements, inside an elevator and at open space were assessed. The bar graphs indicate specific absorption rate values, whereas the line plots represent temperature data.

At this chart peak values occur when the phone is in the tilted position on computational human Pregnant II, configuration 2 for both electromagnetic energy absorption over 10 g and thermal measurements. Raised values are also noticed for configurations 1 and 3. For the fetus, the maximum electromagnetic power density over 10 g and Tmax values at 1000 MHz are found at human configuration 2, at tilt phone position for both open-air setting and the interior environment of the elevator cabin. In essence, the absorbed energy rate over 10 g and peak thermal distributions of fetus are very similar to those of the Pregnant II figure. Both Pregnant II and fetus maximum values are found at the configuration of the models' number three and at tilt phone position, and minimum values are found at cheek position of the handset and computational human configuration 6.

5.1.2. Cell Phone Transmission Frequency of 1800 MHz (SAR10g &Tmax)

For the child, Roberta, the absorption intensity over 10 g analytical results and heat changes under 1800 MHz mobile frequency, are graphically presented in Figure 8.

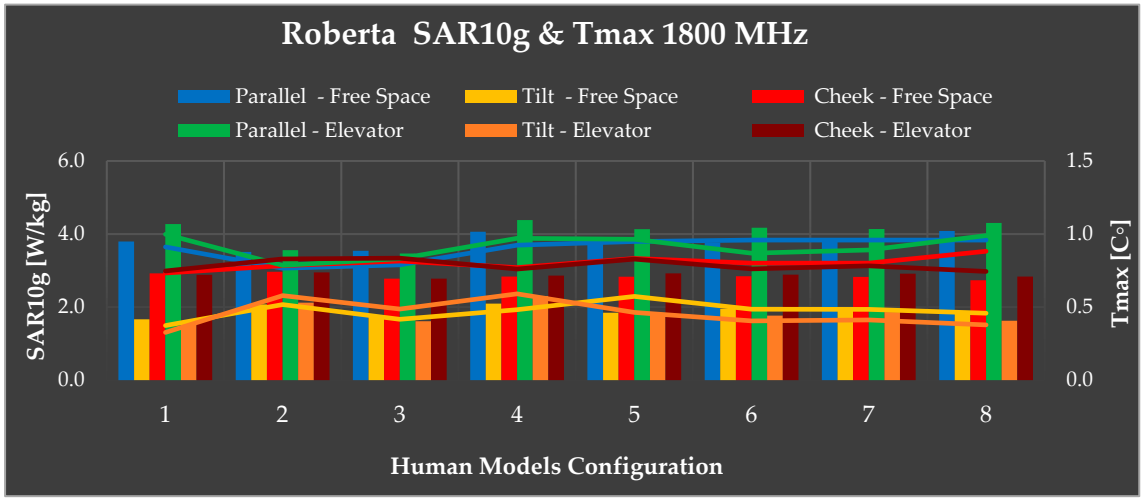



**Figure 8.** Chart display of SAR10g [W/kg] and peak temperature increase (Tmax) [°C] values in the Roberta model at 1800 MHz with the cellphone operating at an output power of 1 W. Eight different anatomical phantom setups and three mobile phone placements, inside an elevator and at open space were assessed. The bar graphs indicate specific absorption rate values, whereas the line plots represent temperature data.

At 1800 MHz, in Roberta the highest local absorption density over 10 g and temperature peak values occur when the mobile phone is used in the vertical position, both in an open environment and enclosed elevator cabin. The tilt placement of the phone, however, results in the lowest peak rate of electromagnetic absorption over 10 g values and the smallest maximum temperature increases in both environments of dosimetry scenarios. Notably, the Tmax values in the vertical position are marginally higher than in the cheek position, in both open-air setting and interior of the elevator cabin.

The maximum electromagnetic dose rate over 10 g value is measured at configuration 8 in free space and at configuration 4 within the elevator cabin. The minimum absorption rate 10 g values at 1800 MHz found at configuration 1 in free space and at configuration 3 inside the elevator cabin. The induced elevation of the temperature reaches its highest value in free space at configuration 1, while inside the elevator cabin, the peak occurs at configuration 8. In both environments, the lowest Tmax is observed in configuration 1.

As far as the Pregnant II and its fetus, respectively, are concerned, in Figures 9 and 10 the specific deposition rate is over 10 g and the Tmax are displayed under the operating condition of 1800 MHz frequency.

Similarly to 1000 MHz case, the maximum absorption rate over 10 g and thermal zenith values for pregnant woman are found at the numerical human's configuration 2 occurring at the tilt placement of the phone, in both open environment and enclosed elevator cabin. The lowest local absorption density over 10 g values is found in parallel phone position, at configuration 7 in free space and at tilt position at configuration 6 inside the elevator cabin. Among the eight configurations of the anatomical replicas, the configurations 1, 2, and 3 consistently result in higher values for the pregnant woman, with the tilt phone position producing higher values compared to the other two positions. Notably, the maximum recorded temperature increases in the two environments is measured in tilt phone position, configuration 2, while the minimum is found at parallel position, configuration 8.

As far as the fetus is concerned, the specific energy absorption over 10 g and Tmax distributions align closely with those at 1000 MHz across all simulation scenarios. The highest tissue energy density over 10 g and Tmax values both occur at configuration 2 in the tilt phone position. The lowest local absorption over 10 g peak and the lowest temperature rise measured at configuration 6, positioned parallel in an open environment and tilted within the elevator cabin.

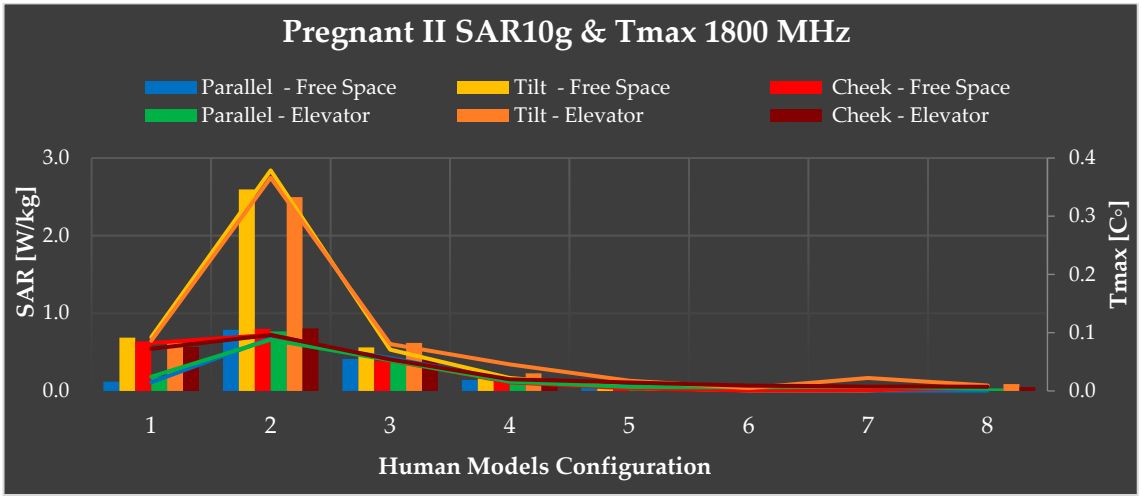



**Figure 9.** Chart display of SAR10g [W/kg] and peak temperature increase (Tmax) [°C] values in the Pregnant II model at 1800 MHz with the cellphone operating at an output power of 1 W. Eight different anatomical phantom setups and three mobile phone placements, inside an elevator and at open space were assessed. The bar graphs indicate specific absorption rate values, whereas the line plots represent temperature data.

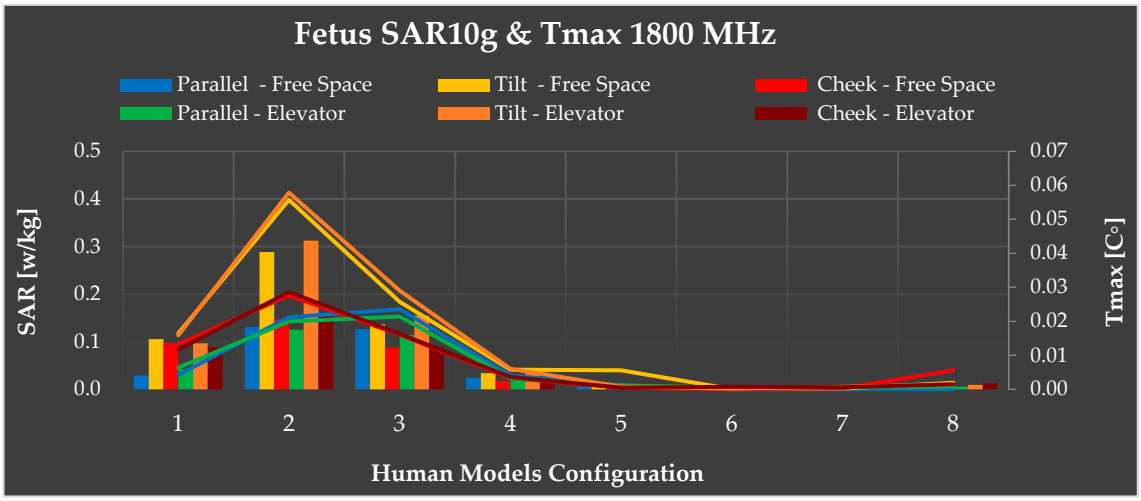



**Figure 10.** Chart display of SAR10g [W/kg] and peak temperature increase (Tmax) [°C] values in the fetus model at 1800 MHz with the cellphone operating at an output power of 1 W. Eight different anatomical phantom setups and three mobile phone placements, inside an elevator and at open space were assessed. The bar graphs indicate specific absorption rate values, whereas the line plots represent temperature data.

### *5.2. Whole Body Specific Absorption Rate—SARwb*

#### 5.2.1. Cell Phone Transmission Frequency of 1000 MHz (SARwb)

The results of the whole-body-specific absorption rate for the child mobile phone user, Roberta, are graphically presented in Figure 11. As seen, the maximum specific absorption

rate of the whole body at 1000 MHz is found at cheek phone position, at configuration 3, under conditions of open space and within the elevator cabin.

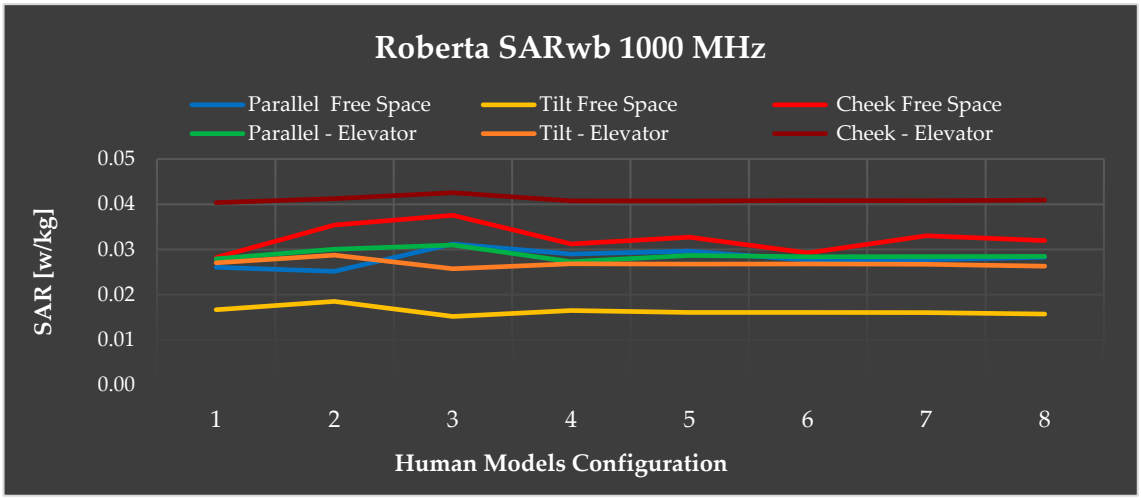



**Figure 11.** Chart displays specific absorption rate of the whole body [W/kg] values in the Roberta model at 1000 MHz with the cellphone operating at an output power of 1 W. Eight different anatomical phantom setups and three portable device placements, inside an elevator and at open space were assessed.

For the anatomical phantom of the pregnant woman, the whole-body RF absorption rate results, are graphically presented on Figure 12. At 1000 MHz, similarly to local absorption coefficient, the highest values can be found at the tilt phone position (configuration 2) in both the free space and the elevator cabin. The lowest of these values can be found at the parallel phone position, configuration 7 both in free space and elevator scenarios.

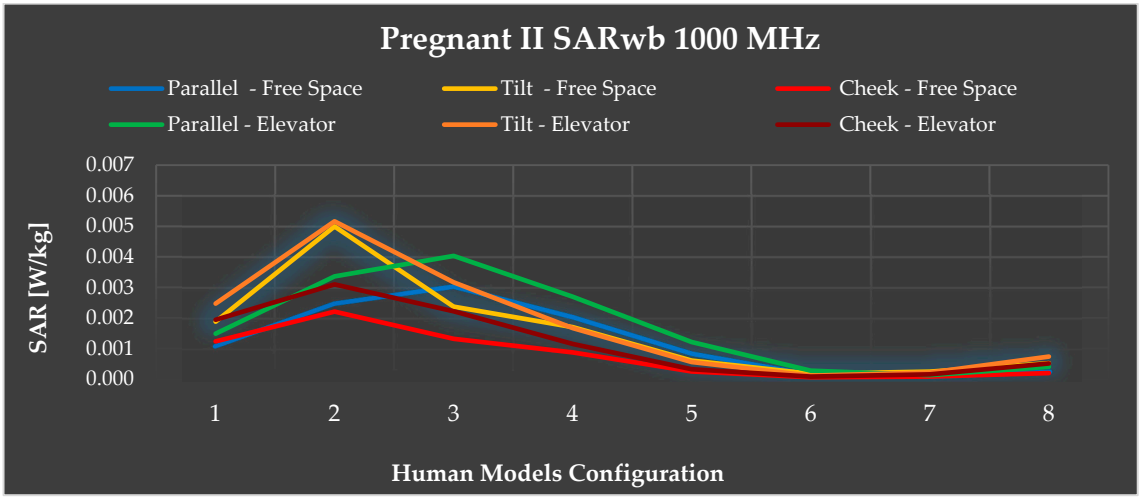



**Figure 12.** The chart displays specific absorption rate of the whole body [W/kg] values in the Pregnant II model at 1000 MHz with the cellphone operating at an output power of 1 W. Eight different anatomical phantom setups and three portable device placements, inside an elevator and at open space were assessed.

The whole-fetus rate of electromagnetic absorption results, shown in Figure 13, present almost the same distribution as the rate of electromagnetic absorption over 10 g and peak temperature point for all the configurations of the performed simulations, in contrast to the Pregnant II model where the distributions of absorption dose rate over 10 g are quite different from those of whole body.

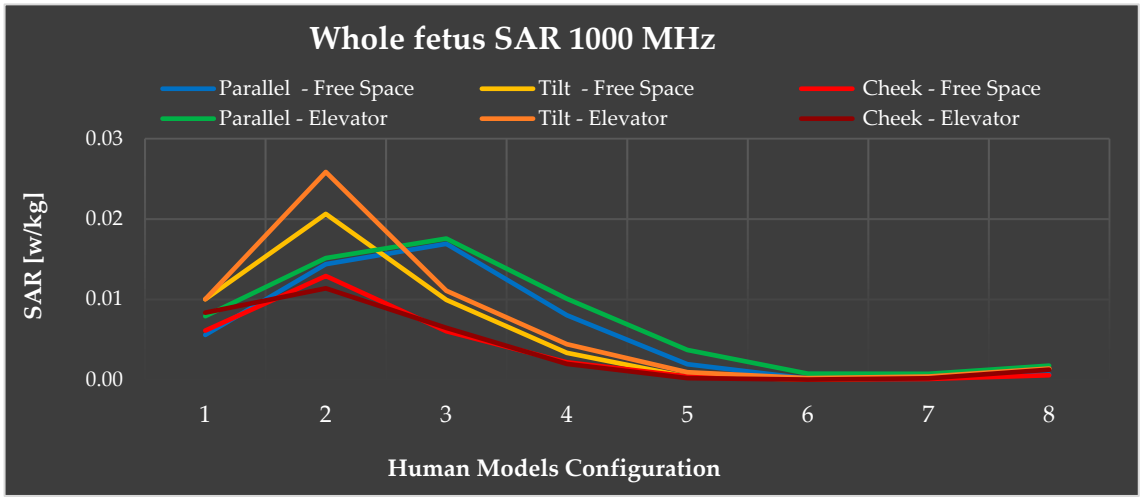



**Figure 13.** Chart displays specific absorption rate of the whole body [W/kg] values in the fetus model at 1000 MHz with the cellphone operating at an output power of 1 W. Eight different anatomical phantom setups and three portable device placements, inside an elevator and at open space were assessed.

5.2.2. Cell Phone Transmission Frequency of 1800 MHz (SARwb)

Results of the whole-body energy absorption for Roberta, Pregnant woman, and fetus are graphically presented in Figures 14–16, respectively.

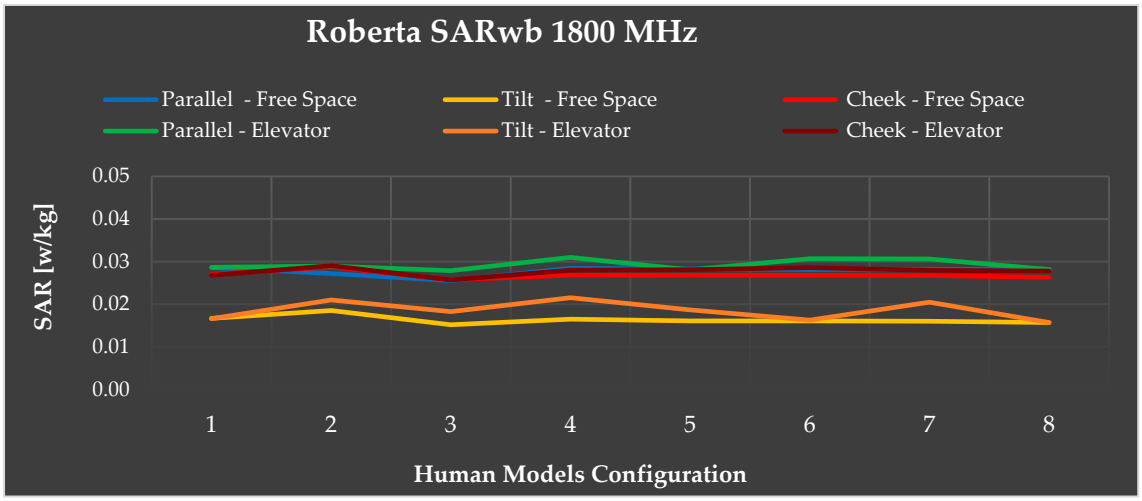



**Figure 14.** Chart displays specific absorption rate of the whole body [W/kg] values in the Roberta model at 1800 MHz with the cellphone operating at an output power of 1 W. Eight different anatomical phantom setups and three portable device placements, inside an elevator and at open space were assessed.

For Roberta, the whole-body specific absorption rate exhibits little variation between parallel and cheek placements of the phone among all considered digital humans' configurations. The highest EM rate of the whole body at 1800 MHz is observed at parallel phone orientation for both simulated environments. In an open environment it is measured at configuration 1 and within the elevator at configuration 6. The minimum value from the calculated maximum measurements of whole-body specific power density is at a tilted orientation of the cell phone for both configurations of open space and metallic enclosure. In free space, whole body specific absorption rate is found at configuration 4, and within the metallic cabin at configuration 6.

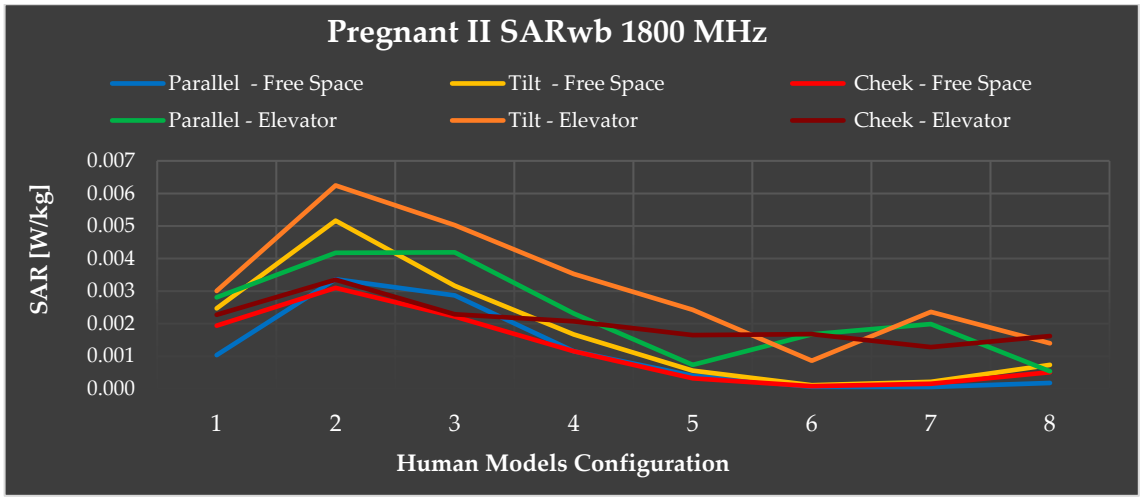



**Figure 15.** Chart displays specific absorption rate of the whole body [W/kg] values in the Pregnant II model at 1800 MHz with the cellphone operating at an output power of 1 W. Eight different anatomical phantom setups and three portable device placements, inside an elevator and at open space were assessed.

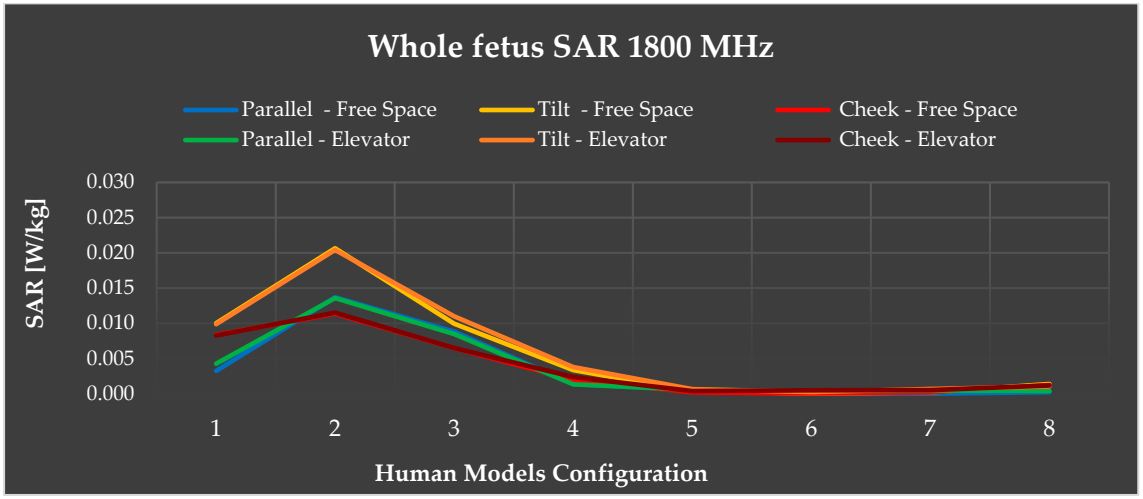



**Figure 16.** Chart displays specific absorption rate of the whole body [W/kg] values in the fetus model at 1800 MHz with the cellphone operating at an output power of 1 W. Eight different anatomical phantom setups and three portable device placements, inside an elevator and at open space were assessed.

The maximum values of the whole-body RF absorption rate for Pregnant woman are found at the orientation tilt of the cell phone, at configuration 2 of the virtual humans, under both free-space and enclosed elevator conditions. The minimum whole-body rate of RF absorption is calculated in the parallel portable device placement at configuration 6 in free space and at configuration 8 in the enclosed cabin area, respectively.

Notably, the whole-fetus electromagnetic energy absorption highest values occur at configuration 2 at the tilted orientation of the handset at both environment configurations. The lowest of the peak whole-body specific absorption rate values is found in the parallel phone position, at configuration 7 in free space and at configuration 6 inside the elevator cabin.

### *5.3. SAR10g Surface Images*

For further analysis and understanding, specific absorption rate over 10 g and maximal temperature surface images of the Pregnant woman are provided for the tilt phone placement, where the highest values across all measurements were recorded for both frequencies

for both the woman and the fetus. The surface patterns are shown with a gradient of black, blue, purple, orange, and yellow, where yellowish white denotes the highest values.

The specific absorption rate of over 10 g surface images (Figure 17) in the provided images is normalized to 1 mW/kg to enhance the visibility of detailed variations. Clearly, the configurations 1, 2, and 3 exhibit the highest values for all dosimetry scenarios. Conversely, in the elevator environment at 1000 MHz operational frequency (Figure 17B), and at 1800 MHz as well (Figure 18B), the specific absorption rate pattern shifts significantly, with minimal representation of black and blue regions, indicating that the lowest specific absorption rate values are nearly absent in this enclosed space.

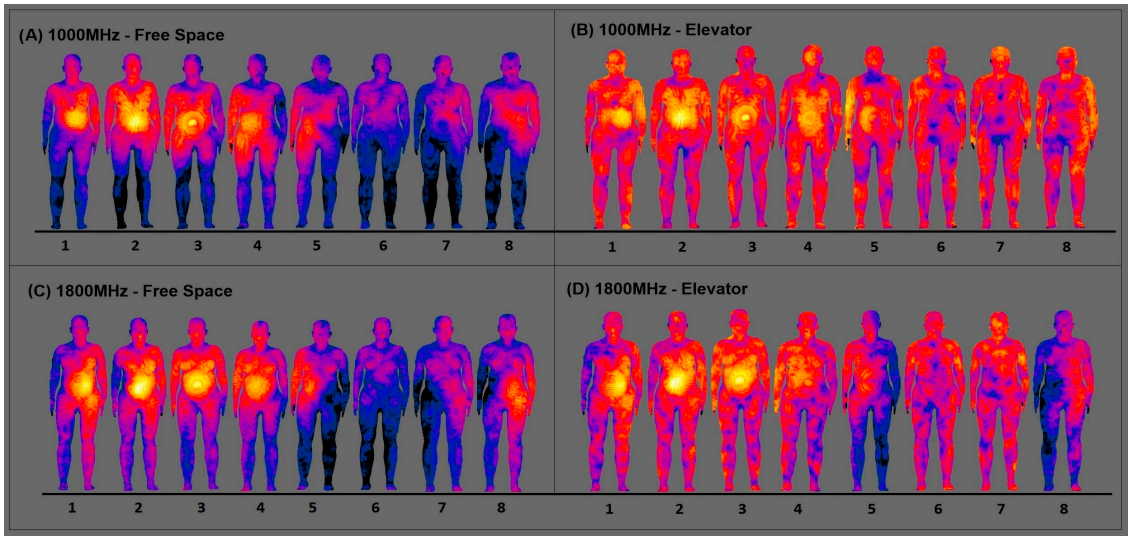



**Figure 17.** Surface image representation of SAR10g [W/kg] normalized over 1 mW/kg, in the Pregnant II model with the cellphone operating at an output power of 1 W, at tilt position and for both frequencies utilized (1000 MHz—(**A**,**B**); 1800 MHz—(**C**,**D**)). Eight virtual subject configurations in free space (**A**,**C**) and within the metallic cabin (**B**,**D**) are presented. Images presented with scaling from 0 dB white color to −50 dB black color. In this view, white through yellow to red marks the hottest, most-exposed spots, magenta through blue indicates moderate to low exposure, and very dark blue or black corresponds to effectively negligible values.

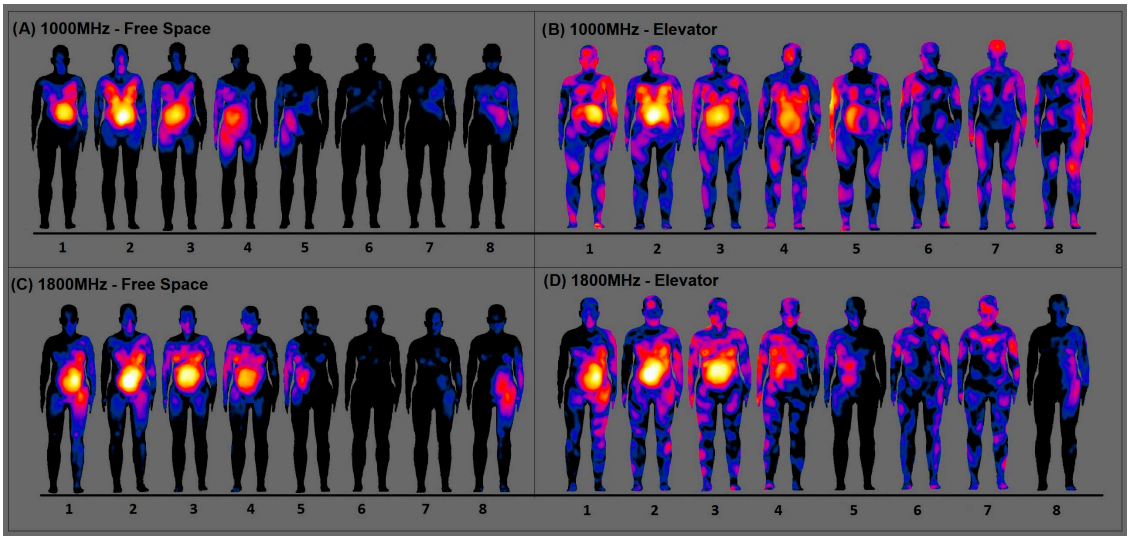



**Figure 18.** Surface image representation of Tmax [°C] increase, normalized over 0.1 °C, in the Pregnant II model with the cellphone operating at an output power of 1 W, at tilt position and for both frequencies utilized (1000 MHz—(**A**,**B**); 1800 MHz—(**C**,**D**)). Eight virtual subject configurations

in free space (**A**,**C**) and within the metallic cabin (**B**,**D**) are presented. Images presented with scaling 0 dB white color to −50 db black color. In this view, white through yellow to red marks the hottest, most-exposed spots, magenta through blue indicates moderate to low exposure, and very dark blue or black corresponds to effectively negligible values.

In the peak thermal surface images, the dB scaling is normalized to a low threshold of 0.1 °C to enable clear detection of minor temperature changes. Like the local absorption density over 10 g images, the Tmax images reveal that the highest temperature increases occur at the configurations of human Figures 1–3 across all configurations. The peak thermal pattern shows that, for certain numerical phantom configurations, temperature increase is minimal, indicated by black areas (no increase) and limited blue areas (indicating a slight increase). The presence of the elevator alters this temperature pattern, producing higher temperature values across the entire body of the digital human in all configurations.

## 6. Discussion

The specific absorption rate over 10 g results indicates that Roberta is more influenced by phone positioning than by the configurations of the virtual humans at both frequencies. Similarly to [55], phone placement is the primary factor affecting variations in specific absorption rate over 10 g, whole body, and highest thermal level for Roberta. Lastly, the metallic cabin elevator increases measured values [53,71] for almost all the configurations of Roberta and the rest of the numerical phantom. In fact, for the human child figurine, Roberta, whole body electromagnetic deposition rate has higher values at the cellphone operating frequency of 1000 MHz than 1800 MHz for most of the simulating scenarios [11]. For both operating frequencies and both experimental environments the maximum temperature is rising to almost 1 °C but does not exceed it [27], and it is found in the ear skin tissue of Roberta. At 1000 MHz, the specific power density over 10 g values is primarily influenced by phone position [12,14,25], and it is increasing as the phone position shifts from a tilt to a parallel orientation and then to the cheek, with only slight variations based on the specific configurations of the virtual human. Additionally, the maximum temperature variations for Roberta are comparable to the absorption dose rate over 10 g values when comparing free space scenarios with similar conditions inside the elevator. However, in this case, the temperature increases from the parallel position to the tilt and then to the cheek position. Lower-frequency EM waves (1000 MHz) reach greater depths than higher-frequency waves (1800 MHz), and that is why at 1000 MHz max values or specific absorption rates over 10 g are found at ear cartilage tissue, and at 1800 MHz they can be found at ear skin tissue under parallel and tilted phone orientations. In the cheek phone position, the maximum SAR10 g values are observed in the muscle tissue at both frequencies. It is evident that the position of the phone affects the tissues involved as the antenna shifts and the placement of the phone on the cheek brings the EM directly to the muscle tissue. When exposed to 1800 MHz in an open environment, Roberta experiences a SAR10g increase when shifting from the tilt to the cheek position, followed by a further rise from cheek to parallel. Also, in most configurations, the energy absorption rate of the whole body for a child phone users is generally higher at 1000 MHz than at 1800 MHz.

While the specific absorption of 10 g and maximal heat point values for Roberta seem to be affected mostly by the orientation of the mobile, for the Pregnant II mannequin, the key factor are the human configurations. Notably, the metallic cabin has an elevated effect on SARwb for Pregnant at 1000 MHz and even more at 1800 MHz. This might be a consequence of the multiple reflections of electromagnetic waves that can spread to the whole cabin and affect the whole body in total, and especially at 1800 MHz, where the wavelength is shorter. Still, SARwb variations are more associated with phone and human figure configurations and less with the inclusion of the metallic structure. As seen, the

human configurations 1, 2, and 3 give the higher values of all measurements for Pregnant II. This is expected since at these three configurations of virtual humans, the Pregnant II model has the closest distance to the portable device [21,31]. Yet, configuration 5 does not have higher values, even though the wireless phone at this configuration is at almost the same distance as configuration number 1. This is happening because Roberta intervenes between the pregnant woman and the cell phone and absorbs the EM radiation. The surface images vividly display the microwave reflections within the metal enclosure and the resulting impact on the exposed human body within these reflections. It is worth mentioning that the presence of the elevator cabin increases measurements, impacting not only the peak values but also measurements in the whole body of Pregnant II. The Tmax pattern closely aligns with the SAR10g surface pattern, showing similar influences from electromagnetic reflections. Distinctively, the presence of the elevator notably alters the electromagnetic absorption rate and temperature distribution patterns.

From the results obtained of the dosimetry study, the graphic distributions of specific absorption rate over 10 g for fetus and Pregnant II have a similar pattern. The highest EM power density over 10 g and highest temperature values across all scenarios taken, for both the pregnant model and the fetus are recorded at configuration 2 with the phone in a tilt position, emphasizing that positioning is the primary factor influencing these exposure levels. The second highest SAR10 values indicate that the positioning of both the digital humans and the phone has a greater impact on absorption rate levels of the fetus than the presence of the elevator itself. While SARwb values are typically low for the fetus, most measurements reveal a noticeable increase in the peak values inside the metallic elevator cabin. The distance between the phone and the fetus, and the interference of other tissues from the figures of Pregnant II and Roberta are the main factors affecting the absorption rate level of the fetus. It should be underlined, that in all studied scenarios, the temperature increase for pregnant women and fetuses remains well below 1 °C, the threshold associated with health issues in animal fetuses, as noted by the WHO [72].

When comparing the results in this work with the previous study [55], differences are noted. For example, in [55], Roberta SAR10g increases as the phone transitions from a parallel position to a tilt and finally to the cheek. In the current study, however, specific absorption rate follows a different pattern, rising from the tilt position to parallel and then to the cheek. In addition, ref. [55] exhibits a higher peak local absorption density at 1000 MHz. Still, Tmax remains nearly identical between the two studies, with significantly higher values at the cheek compared to the tilt and parallel positions. Additionally, the maximum and minimum values across both studies are closely aligned. At 1800 MHz, both SAR10g and Tmax follow the same trends, with identical maximum and minimum values occurring at the same phone positions. As far as SARwb is concerned, similar values and distribution in both studies for Roberta are calculated. Even if higher SARwb is found in some measurements than [55], the differences are very small, and the values match each other.

In contrast to Roberta's calculations regarding the gestational body, the highest EM absorption intensity and maximum thermal intensity values at 1000 MHz are found in the same configuration for both studies; that is, when the handset is in a tilt position and when the distance between the child and the pregnant numerical phantom is minimized. Yet, in this study, the peak SAR and Tmax values are higher than those in the previous study [55]. Furthermore, the whole-body specific absorption rate for pregnant women is influenced by the portable telecommunication device position and also by human position, while in [55] it is influenced mostly by phone position. The values here are also similar to each other in the two studies.

Finally, for fetal exposure, this study finds higher maximum values across all frequencies as compared to a previous study [55]. The distribution pattern mirrors that of the Pregnant II model, whereas in a previous study [55], it differed. Notably, in both studies, all fetal maximum values are concentrated in the amniotic fluid.

## 7. Conclusions

A comprehensive investigation into electromagnetic (EM) exposure and thermal safety has been conducted, focusing on three distinct subjects: a girl of five years named Roberta, a gestating female at seven months gestation known as Pregnant II, and her fetus. This study employed anatomically precise computational virtual humans along with a cellular device functioning at two different frequency bands, 1000 MHz and 1800 MHz. A total of 48 separate arrangements involving these numerical phantoms in various configurations and with different phone orientations were meticulously analyzed. The study presented detailed results of SAR10g, SAR-wb, and Tmax for every anatomical virtual human, including the fetus within the confines of an elevator cabin. The results here add to the findings in our prior work [55]. Here, contrary to [55], we examined how exactly, and in which scale, the positioning of the humans affects the quantities measured for all the utilized models, including the seven-month fetus.

Notably, it becomes evident that an integrated approach is essential to fully understand the complexities of EM exposure. Each configuration offers unique insights into how specific absorption rate values and temperature rises differ across subjects and settings. The variations observed underscore the necessity of examining every possible configuration to draw comprehensive conclusions about EM safety.

Moreover, the investigation highlights the importance of further exploring the effects of EM exposure in elevator cabins under various occupancy conditions and at different portable device frequencies. Such studies are crucial for developing targeted safety guidelines and protective measures, particularly in environments where RF exposure is compounded by enclosed spaces like elevators. This research not only enhances our understanding of EM field interactions with human tissues but also aids in the formulation of better health and safety standards for vulnerable populations such as children and pregnant women.

**Author Contributions:** Conceptualization, I.K.; Methodology, I.K.; Software, I.K.; Formal analysis, I.K.; Resources, I.K.; Data curation, I.K.; Writing—original draft preparation, I.K.; Writing—review & editing, S.B. and S.K.; Supervision, S.K. All authors have read and agreed to the published version of the manuscript.

**Funding:** This research received no external funding.

**Data Availability Statement:** The original contributions presented in this study are included in the article. Further inquiries can be directed to the corresponding author.

**Conflicts of Interest:** The authors declare no conflict of interest.

## References

1. Hossain, M.I.; Faruque, M.R.I.; Islam, M.T. Analysis on the effect of the distances and inclination angles between human head and mobile phone on SAR. *Prog. Biophys. Mol. Biol.* **2015**, *119*, 103–110. [CrossRef] [PubMed]
2. Takei, R.; Nagaoka, T.; Saito, K.; Watanabe, S.; Takahashi, M. SAR variation due to exposure from a smartphone held at various positions near the torso. *IEEE Trans. Electromagn. Compat.* **2017**, *59*, 747–753. [CrossRef]
3. Li, Y.; Lu, M. Study on SAR distribution of electromagnetic exposure of 5G mobile antenna in human brain. *J. Appl. Sci. Eng.* **2020**, *23*, 279–287.
4. Wang, H.H. Analysis of electromagnetic energy absorption in the human body for mobile terminals. *IEEE Open J. Antennas Propag.* **2020**, *1*, 113–117. [CrossRef]

5. Ben Hamadi, H.; Ghnimi, S.; Latrach, L.; Benech, P.; Gharsallah, A. New design of multi-band PIFA antenna with reduced SAR for mobile and wireless applications. *Wirel. Pers. Commun.* **2020**, *115*, 1211–1226. [CrossRef]
6. Karim, M.E.; Hossain, B.M.A. SAR analysis of human head model using common antennas of 4G LTE mobile communications. In Proceedings of the Fourth International Conference on Electrical, Computer and Communication Technologies (ICECCT), Erode, India, 15–17 September 2021.
7. Bonato, M.; Dossi, L.; Gallucci, S.; Benini, M.; Tognola, G.; Parazzini, M. Assessment of human exposure levels due to mobile phone antennas in 5G networks. *Int. J. Environ. Res. Public Health* **2022**, *19*, 1546. [CrossRef] [PubMed]
8. Ramachandran, T.; Faruque, M.R.I.; Islam, M.T. Specific absorption rate reduction for sub-6 frequency range using polarization dependent metamaterial with high effective medium ratio. *Sci. Rep.* **2022**, *12*, 1803. [CrossRef] [PubMed]
9. Takasaka, C.; Saito, K.; Takahashi, M.; Nagaoka, T.; Wake, K. Specific absorption rate (SAR) calculations in the abdomen of the human body caused by smartphone at various tilt angles: A consideration of the 1950 MHz band. *IEICE Trans. Commun.* **2022**, *E105-B*, 295–301. [CrossRef]
10. Zhang, H.H.; Gong, L.F.; Wang, J.; Sha, W.E.I.; Li, L.; Wang, J.X.; Wang, C. Specific absorption rate assessment of fifth generation mobile phones with specific anthropomorphic mannequin model and high-resolution anatomical head model. *Int. J. RF Microw. Comput.-Aided Eng.* **2022**, *32*, e23158. [CrossRef]
11. Yi, M.; Chi, Y.; Wu, B.; Zhao, Y.; Su, T.; Qi, Y. Safety assessment of electromagnetic radiation from mobile phone antennas to the human head. *Int. J. Energy* **2023**, *2*, 23–26. [CrossRef]
12. Turgut, A.; Engiz, B.K. Analyzing the SAR in human head tissues under different exposure scenarios. *Appl. Sci.* **2023**, *13*, 6971. [CrossRef]
13. Lee, A.K.; Hong, S.E.; Kwon, J.H.; Choi, H.D. SAR comparison of SAM phantom and anatomical head models for a typical bar-type phone model. *IEEE Trans. Electromagn. Compat.* **2015**, *57*, 1281–1284. [CrossRef]
14. Vieira, V.F.; Pessoa, L.M.; Carvalho, M.I. Evaluation of SAR induced by a planar inverted-F antenna based on a realistic human model. In Proceedings of the Joint Conference of EMBEC and NBC, Tampere, Finland, 11–15 June 2017.
15. Rani, M.U.; Baba, V.S.S.N.S.; Gundala, S. Analysis of SAR in human blood, bones and muscles due to mobile waves at 900 MHz, 1800 MHz and 2400 MHz. *Int. J. Appl. Eng. Res.* **2018**, *13*, 2125–2129.
16. Chowdhury, A.; Paul, N.; Islam, S.S.; Hossain, M.I. Comparison of electromagnetic absorption in human head for dipole and microstrip patch antenna. In Proceedings of the International Conference on Innovations in Science, Engineering and Technology (ICISET), Chittagong, Bangladesh, 27–28 October 2018.
17. Mumin, A.R.O.; Alias, R.; Abdullah, J.; Dahlan, S.H.; Ali, J. Assessment of electromagnetic absorption towards human head using specific absorption rate. *Bull. Electr. Eng. Inform.* **2018**, *7*, 657–664.
18. Mahmud, S. Analysis of mobile phone radiation effect on human body using specific absorption rate. *Asian J. Appl. Sci. Eng.* **2022**, *11*, 7–19. [CrossRef]
19. Lee, A.K.; Hong, S.E.; Kwon, J.H.; Choi, H.D.; Cardis, E. Mobile phone types and SAR characteristics of the human brain. *Phys. Med. Biol.* **2017**, *62*, 2741–2761. [CrossRef] [PubMed]
20. Elyamani, A.F.; Cueille, M.; Castagnetti, A.; Peyrard, P.; Villeneuve, R.; Amblard, R.; Garnier, N.; Serrano, B.; Dubard, J.-L. Influence of morphology and tissue distribution on SAR estimation: Application on a heterogeneous head with realistic connected glasses. In Proceedings of the International Workshop on Antenna Technology (iWAT), Bucharest, Romania, 25–28 February 2020.
21. Sallomi, A.H.; Ahmed, G.A. Simulating the specific absorption rates in different human tissues at 4G frequencies for mobile phones. *Bull. Electr. Eng. Inform.* **2023**, *12*, 2860–2869. [CrossRef]
22. Wessapan, T.; Rattanadecho, P. Temperature induced in human organs due to near-field and far-field electromagnetic exposure effects. *Int. J. Heat Mass Transf.* **2018**, *119*, 65–76. [CrossRef]
23. Kaburcuk, F.; Elsherbeni, A. Temperature rise and SAR distribution at wide range of frequencies in a human head due to an antenna radiation. *Appl. Comput. Electromagn. Soc. J. ACES* **2018**, *33*, 367–372.
24. Zhang, H.H.; Lin, Z.C.; Sha, W.E.I.; Choi, W.W.; Tam, K.W.; Donoro, D.G.; Shi, G. Electromagnetic-Thermal Analysis of Human Head Exposed to Cell Phones With the Consideration of Radiative Cooling. *IEEE Antennas Wirel. Propag. Lett.* **2018**, *17*, 1584–1587. [CrossRef]
25. Cavagnaro, M.; Lin, J.C. Importance of Exposure Duration and Metrics on Correlation Between RF Energy Absorption and Temperature Increase in a Human Model. *IEEE Trans. Biomed. Eng.* **2019**, *66*, 2253–2258. [CrossRef] [PubMed]
26. Laissaoui, A.; Mezouad, S.; Nekhoul, B. SAR Evalution in Human Head Exposed to RF Radiation. In Proceedings of the International Conference on Advances in Electrical Engineering (ICAEE), Constantine, Algeria, 29–31 October 2022.
27. Seetharaman, R.; Tharun, M.; Gayathri, S.; Mole, S.S.S.; Anandan, K. Analysis of specific absorption rate and heat transfer in human head due to mobile phones. *Mater. Today Proc.* **2022**, *51*, 2365–2374. [CrossRef]
28. Ramadan, A.; Shafey, H.; Abdelshafe, N.; Abdel-Rahman, A.K. Realistic Computational Modeling of Biothermal Effects Inside Human Head Exposed to Mobile Phone Radiation. *J. Eng. Sci.* **2023**, *51*, 16–36. [CrossRef]
29. Siriwitpreecha, A.; Rattanadecho, P.; Wessapan, T. The influence of wave propagation mode on specific absorption rate and heat transfer in human body exposed to electromagnetic wave. *Int. J. Heat Mass Transf.* **2013**, *65*, 423–434. [CrossRef]

30. Joukar, A.; Nammakie, E.; Niroomand-Oscuii, H. A comparative study of thermal effects of 3 types of laser in eye: 3D simulation with bioheat equation. *J. Therm. Biol.* **2015**, *49*, 74–81. [CrossRef] [PubMed]
31. Wessapan, T.; Rattanadecho, P. Temperature induced in the testicular and related tissues due to electromagnetic fields exposure at 900 MHz and 1800 MHz. *Int. J. Heat Mass Transf.* **2016**, *102*, 1130–1140. [CrossRef]
32. Stankovic, V.; Jovanovic, D.; Krstic, D.; Markovic, V.; Cvetkovic, N. Temperature distribution and Specific Absorption Rate inside a child's head. *Int. J. Heat Mass Transf.* **2017**, *104*, 559–565. [CrossRef]
33. Lwin, Z.M.; Yokota, M. Numerical analysis of SAR and temperature distribution in two dimensional human head model based on FDTD parameters and the polarization of electromagnetic wave. *AEU-Int. J. Electron. Commun.* **2019**, *104*, 91–98. [CrossRef]
34. Bhargava, D.; Rattanadecho, P.; Wessapan, T. The effect of metal objects on the SAR and temperature increase in the human head exposed to dipole antenna (numerical analysis). *Case Stud. Therm. Eng.* **2020**, *22*, 100789. [CrossRef]
35. Gandhi, O.P.; Morgan, L.L.; de Salles, A.A.; Han, Y.-Y.; Herberman, R.B.; Davis, D.L. Exposure limits: The underestimation of absorbed cell phone radiation, especially in children. *Electromagn. Biol. Med.* **2012**, *31*, 34–51. [CrossRef] [PubMed]
36. Deepika, B.; Ramya, V.; Yamuna, T.; Kalpana, R. A numerical analysis of temperature distribution in human eye when exposed to electromagnetic radiation. In Proceedings of the IEEE International Conference on Electronics, Computing and Communication Technologies (CONECCT), Bangalore, India, 10–11 July 2015.
37. Lee, A.-K.; Park, J.S.; Hong, S.-E.; Taki, M.; Wake, K.; Wiart, J.; Choi, H.D. Brain SAR of average male Korean child to adult models for mobile phone exposure assessment. *Phys. Med. Biol.* **2019**, *64*, 045004. [CrossRef] [PubMed]
38. Wang, J.; Mu, S.; Hai, Z. Research on the Influence of Electromagnetic Radiation in the Automobile on the SAR Value of Human Body. In Proceedings of the International Seminar on Artificial Intelligence, Networking and Information Technology (AINIT 2020), Shanghai Institute of Technology, Shanghai, China, 18–20 September 2020.
39. Birks, L.E.; Van Wel, L.; Liorni, I.; Pierotti, L.; Guxens, M.; Huss, A.; Foerster, M.; Capstick, M.; Eeftens, M.; El Marroun, H.; et al. Radiofrequency electromagnetic fields from mobile communication: Description of modeled dose in brain regions and the body in European children and adolescents. *Environ. Res.* **2021**, *193*, 110505. [CrossRef] [PubMed]
40. Ahmed, G.A.; Sallomi, A.H. SAR Calculation in a Child Seven-Layer Head Model at 2.1 and 2.6 GHz. *Wasit J. Comput. Math. Sci.* **2023**, *2*, 62–71. [CrossRef]
41. Hadjem, A.; Conil, E.; Gati, A.; Wong, M.-F.; Wiart, J. Analysis of power absorbed by children's head as a result of new usages of mobile phone. *IEEE Trans. Electromagn. Compat.* **2010**, *52*, 812–819. [CrossRef]
42. Fernández, C.; de Salles, A.A.; Sears, M.E.; Morris, R.D.; Davis, D.L. Absorption of wireless radiation in the child versus adult brain and eye from cell phone conversation or virtual reality. *Environ. Res.* **2018**, *167*, 694–699. [CrossRef] [PubMed]
43. Bhargava, D.; Leeprechanon, N.; Rattanadecho, P.; Wessapan, T. Specific absorption rate and temperature elevation in the human head due to overexposure to mobile phone radiation with different usage patterns. *Int. J. Heat Mass Transf.* **2019**, *130*, 1178–1188. [CrossRef]
44. Sudan, M.; Birks, L.E.; Aurrekoetxea, J.J.; Ferrero, A.; Gallastegi, M.; Guxens, M.; Ha, M.; Lim, H.; Olsen, J.; González-Safont, L.; et al. Maternal cell phone use during pregnancy and child cognition at age 5 years in 3 birth cohorts. *Environ. Int.* **2018**, *120*, 155–162. [CrossRef] [PubMed]
45. Boileau, N.; Margueritte, F.; Gauthier, T.; Boukeffa, N.; Preux, P.-M.; Labrunie, A.; Aubard, Y. Mobile phone use during pregnancy: Which association with fetal growth? *J. Gynecol. Obstet. Hum. Reprod.* **2020**, *49*, 101852. [CrossRef] [PubMed]
46. Bektas, H.; Dasdag, S.; Bektas, M.S. Comparison of effects of 2.4 GHz Wi-Fi and mobile phone exposure on human placenta and cord blood. *Biotechnol. Biotechnol. Equip.* **2020**, *34*, 154–162. [CrossRef]
47. Sandeep, S.; Vard, A.; Guxens, M.; Bloch, I.; Wiart, J. RF-EMF Exposure Assessment of Fetus During the First Trimester of Pregnancy. *IEEE Access* **2024**, *12*, 75311–75322. [CrossRef]
48. Psenakova, Z.; Beňová, M.; Lauková, T. Investigation of Specific absorption rate (SAR) near model of fetus in uterus. In Proceedings of the IEEE International Conference ELEKTRO, Taormina, Italy, 25–28 May 2020.
49. Bektas, H.; Dasdag, S.; Bektas, M.S. Evaluation of 900 and 1800 MHz Radiofrequency Radiation Emitted from Mobile Phones on Pregnant Women. *J. Int. Dent. Med. Res.* **2021**, *14*, 1675–1683.
50. Karatsi, I.; Bakogianni, S.; Koulouridis, S. Temperature variations for adults and child human models inside elevator cabin. In Proceedings of the IEEE International Symposium on Antennas and Propagation (APSURSI), Fajardo, PR, USA, 26 June–1 July 2016.
51. Salah, I.Y.; Khalil, Y.A. High Resolution Numerical Modelling of In-Vehicle Mobile Cars. *Int. J. Electromagn. Appl.* **2015**, *5*, 66–72.
52. Gombarska, D.; Smetana, M.; Janousek, L. High-Frequency Electromagnetic Field Measurement Inside Personal Vehicle Within Urban Environment. In Proceedings of the 12th International Conference on Measurement (MEASUREMENT), Smolenice, Slovakia, 27–29 May 2019.
53. Psenakova, Z.; Benova, M.; Mydlova, J. Investigation of SAR (Specific Absorption Rate) in Different Head Models Placed in Shielded Space. In Proceedings of the IEEE 20th International Conference on Computational Problems of Electrical Engineering (CPEE), Lviv-Slavske, Ukraine, 15–18 September 2019.

54. Benova, M.; Mydlova, J.; Psenakova, Z.; Smondrk, M. SAR evaluation in human head models with cochlear implant near PIFA antenna inside a railway vehicle. In *Information Technology in Biomedicine*, 1st ed.; Springer: Cham, Switzerland, 2020; pp. 289–300, ISBN 9783030496654/9783030496661.
55. Karatsi, I.; Bakogianni, S.; Koulouridis, S. SAR and Thermal Distribution of Pregnant Woman and Child Inside Elevator Cabin. *Int. J. Microw. Wirel. Technol.* **2022**, *15*, 213–226. [CrossRef]
56. Schmid & Partner Engineering AG. Available online: http://www.speag.com/speag (accessed on 10 July 2025).
57. Sonawane, A.D.; Bormane, D.S. A Specific Absorption Rate in Human Head due to Mobile Phone Radiations: Review. In Proceedings of the International Conference on Electronics and Sustainable Communication Systems (ICESC), Coimbatore, India, 2–4 July 2020.
58. Pinto, Y.C.; Ghanmi, A.; Hadjem, A.; Conil, E.; Namur, T.; Person, C.; Wiart, J. Numerical Mobile phone models validated by SAR measurements. In Proceedings of the 5th European Conference on Antennas and Propagation (EUCAP), Rome, Italy, 10–15 April 2011.
59. *IEEE/IEC 62209-1528-2020*; IEC/IEEE International Standard—Measurement Procedure for the Assessment of Specific Absorption Rate of Human Exposure to Radio Frequency Fields from Hand-Held and Body-Mounted Wireless Communication Devices–Part 1528: Human Models, Instrumentation, and Procedures (Frequency Range of 4 MHz to 10 GHz). International Electrotechnical Commission: Geneva, Switzerland, 2020.
60. *IEC EN62209-2:2010*; Human Exposure to Radio Frequency Fields from Hand-Held and Body-Mounted Wireless Communication Devices. Human Models, Instrumentation, and Procedures. Part 2: Procedure to Determine the Specific Absorption Rate (SAR) for Wireless Communication Devices Used in Close Proximity to the Human Body (Frequency Range of 30 MHz to 6 GHz). International Electrotechnical Commission: Geneva, Switzerland, 2010; ISBN 978-2-88910-642-4.
61. *IEEE C95.1-2019/Cor 2-2020*; IEEE Standard for Safety Levels with Respect to Human Exposure to Electric, Magnetic, and Electromagnetic Fields, 0 Hz to 300 GHz–Corrigenda 2, 2019–2020. Institute of Electrical and Electronics Engineers: Piscataway Township; NJ, USA, 2020.
62. International Commission on Non-Ionizing Radiation Protection (ICNIRP). Guidelines for Limiting Exposure to Electromagnetic Fields (100 kHz to 300 GHz). In *ICNIRP Guidelines*; The International Commission on Non-Ionizing Radiation Protection: Munich, Germany, 2020.
63. Pennes, H.H. Analysis of tissue and arterial blood temperatures in resting forearm. *J. Appl. Physiol.* **1948**, *1*, 93–122. [CrossRef] [PubMed]
64. Christ, A.; Guldimann, R.; Buhlmann, B.; Zefferer, M.; Bakker, J.F.; Van Rhoon, G.C.; Kuster, N. Exposure of the human body to professional and domestic induction cooktops compared to the basic restrictions. *Bioelectromagnetics* **2012**, *33*, 695–705. [CrossRef] [PubMed]
65. Fiocchi, S.; Parazzini, M.; Liorni, I.; Samaras, T.; Ravazzani, P. Temperature Increase in the Fetus Exposed to UHF RFID Readers. *IEEE Trans. Biomed. Eng.* **2014**, *61*, 2011–2019. [CrossRef] [PubMed]
66. Bakker, J.F.; Paulides, M.M.; Neufeld, E.; Christ, A.; Kuster, N.; Van Rhoon, G.C. Children and adults exposed to electromagnetic fields at the ICNIRP reference levels: Theoretical assessment of the induced peak temperature increase. *Phys. Med. Biol.* **2011**, *56*, 4967–4989. [CrossRef] [PubMed]
67. Gosselin, M.-C.; Neufeld, E.; Moser, H.; Huber, E.; Farcito, S.; Gerber, L.; Jedensjö, M.; Hilber, I.; Di Gennaro, F.; Lloyd, B.; et al. Development of a New Generation of High-Resolution Anatomical Models for Medical Device Evaluation: The Virtual Population 3.0. *Phys. Med. Biol.* **2014**, *59*, 5287. [CrossRef] [PubMed]
68. Government Gazette of the Hellenic Republic. Issue A, No. 79 (9 April 2012). Law No. 4067, New Building Regulation. Available online: http://www.publicrevenue.gr/elib/view?d=/gr/act/2012/4067/main/art/27/ (accessed on 10 July 2025).
69. Hellenic Accreditation System. ESYD KO-ANEL/01/06/14-11-2017 2/161. Edition 01; Revision 06; Issue Date 26 May 2004; Revision Date 14 November 2017. Available online: http://esydops.gr/pweb/s/20/files/kanonismoi/kritiriaOdigies/ko_anel_14_11_2017.pdf (accessed on 10 July 2025).
70. *IEEE standard 1528*; IEEE Recommended Practice for Determining the Peak Spatial-Average Specific Absorption Rate (SAR) in the Human Head from Wireless Communications Devices: Measurement Techniques. Institute of Electrical and Electronics Engineers: Piscataway Township, NJ, USA, 2013.
71. Karatsi, I.; Koulouridis, S. Dosimetry Study of Anatomical Pregnant Woman & Fetus Models Inside Three Different Elevator Cabins. In Proceedings of the 9th European Conference on Antennas and Propagation (EuCAP), Lisbon, Portugal, 13–17 April 2015.
72. World Health Organization (WHO). *Environmental Health Criteria 137: Electromagnetic Fields (300 kHz to 300 GHz)*; World Health Organization (WHO): Geneva, Switzerland, 1993.


**Disclaimer/Publisher's Note:** The statements, opinions and data contained in all publications are solely those of the individual author(s) and contributor(s) and not of MDPI and/or the editor(s). MDPI and/or the editor(s) disclaim responsibility for any injury to people or property resulting from any ideas, methods, instructions or products referred to in the content.